

# Scale-invariant magnetic anisotropy in $\alpha$ -RuCl<sub>3</sub>: A quantum Monte Carlo study

Toshihiro Sato,<sup>1,2,3</sup> B. J. Ramshaw,<sup>4,5</sup> K. A. Modic,<sup>6</sup> and Fakhri F. Assaad<sup>3,2</sup>

<sup>1</sup>*Institute for Theoretical Solid State Physics, IFW Dresden, 01069 Dresden, Germany*

<sup>2</sup>*Würzburg-Dresden Cluster of Excellence ct.qmat, Germany*

<sup>3</sup>*Institut für Theoretische Physik und Astrophysik, Universität Würzburg, 97074 Würzburg, Germany*

<sup>4</sup>*Laboratory of Atomic and Solid State Physics, Cornell University, Ithaca, New York 14853, USA*

<sup>5</sup>*Canadian Institute for Advanced Research, Toronto, Ontario, Canada*

<sup>6</sup>*Institute of Science and Technology Austria, 3400 Klosterneuburg, Austria*

We compute the rotational anisotropy of the free energy of  $\alpha$ -RuCl<sub>3</sub> in an external magnetic field. This quantity, known as the magnetotropic susceptibility,  $k$ , relates to the second derivative of the free energy with respect to the angle of rotation. We have used approximation-free, auxiliary-field quantum Monte Carlo simulations for a realistic model of  $\alpha$ -RuCl<sub>3</sub> and optimized the path integral to alleviate the negative sign problem. This allows us to reach temperatures down to 30 K—an energy scale below the dominant Kitaev coupling. We demonstrate that the magnetotropic spin susceptibility in this model of  $\alpha$ -RuCl<sub>3</sub> displays scaling behavior  $k = Tf(B/T)$  at high temperatures. Once the uniform susceptibility departs from the Curie law (i.e., at the energy scale of the exchange interactions), it appears to transition to an emergent scalinglike behavior, characterized by a different function  $f$  at lower temperatures, stemming from the locality of torque fluctuations. We observe a remarkable numerical match between experiment and simulations and we also find qualitative agreement with the pure Kitaev model. In comparison, for the XXZ Heisenberg Hamiltonian, the scaling  $k = Tf(B/T)$  breaks down at a temperature scale where the uniform spin susceptibility deviates from the Curie law and never reemerges at low temperatures.

*Introduction.* Quantum spin liquids are believed to harbor exotic fractionalized excitations that defy the conventional categories of fermions and bosons. The Kitaev model, originally proposed by Kitaev in 2006 [1], has served as a paradigm in this context, offering an exact solution for a quantum spin liquid state on the honeycomb lattice.

$\alpha$ -RuCl<sub>3</sub> has emerged as a leading candidate for realizing the Kitaev spin liquid [2–4]. Numerous experiments have probed its thermodynamic and dynamical properties and have reached the conclusion that there is a large Kitaev exchange interaction [5–15]. One intriguing observation is the emergence of scale invariance at low temperatures and in high magnetic fields [16]. The aim of this Letter is to bridge this experimental observation in  $\alpha$ -RuCl<sub>3</sub> with approximation-free finite temperature numerical simulations. Using minimal models to describe  $\alpha$ -RuCl<sub>3</sub> we will see that there is a domain of temperatures and magnetic fields where numerics and experiments agree quantitatively. With the numerical approach we can probe higher magnetic fields than accessible in the laboratory, thereby suggesting the presence of two separate scaling regimes, each associated with a different scaling function. While the high temperature regime is generic to all spin models and emerges at scales well above the magnetic exchange scale, the lower scaling regime is characteristic of materials proximate to the Kitaev model.

*Minimal models for Kitaev materials.* We consider first-neighbor, Kitaev  $K_1$ , and off-diagonal symmetric,  $\Gamma_1$ , couplings, as well as first-neighbor (third-neighbor)

Heisenberg couplings,  $J_1$  ( $J_3$ ), on the honeycomb lattice:

$$\hat{H}_s = \sum_{i \in A, \gamma} \left[ K_1 \hat{S}_i^\gamma \hat{S}_{i+\delta_\gamma}^\gamma + \Gamma_1 \left( \hat{S}_i^\alpha \hat{S}_{i+\delta_\gamma}^\beta + \hat{S}_i^\beta \hat{S}_{i+\delta_\gamma}^\alpha \right) \right] + \sum_{i \in A, \delta_\gamma} J_1 \hat{S}_i \cdot \hat{S}_{i+\delta_\gamma} + \sum_{i \in A, \delta'_\gamma} J_3 \hat{S}_i \cdot \hat{S}_{i+\delta'_\gamma}. \quad (1)$$

Here  $i$  runs over the  $A$  sublattice and  $i + \delta_\gamma$  ( $i + \delta'_\gamma$ ) over the first (third) neighbors. For the first term  $(\gamma, \alpha, \beta) = (1, 2, 3)$  for the  $X$  bonds,  $(\gamma, \alpha, \beta) = (2, 3, 1)$  for the  $Y$  bonds, and  $(\gamma, \alpha, \beta) = (3, 1, 2)$  for the  $Z$  bonds on each lattice site [see Fig. 1(a)].

To study the magnetotropic susceptibility of  $\alpha$ -RuCl<sub>3</sub> under high magnetic fields reported in Ref. [16], we add a Zeeman term to produce the total Hamiltonian

$$\hat{H} = \hat{H}_s - \mu_B \sum_i \mathbf{B} \cdot \hat{g} \cdot \hat{S}_i, \quad (2)$$

where the direction of the magnetic field in the cubic spin basis corresponds to  $\mathbf{B} || [xyz]$  [see Fig. 1(a)]. In Kitaev materials such as  $\alpha$ -RuCl<sub>3</sub>, the [111] axis aligns with the  $\mathbf{c}$  axis, perpendicular to the honeycomb lattice, whereas the [11 $\bar{2}$ ] and [ $\bar{1}$ 10] axes correspond to the in-plane  $\mathbf{a}$  and  $\mathbf{b}$  axes, respectively [see Fig. 1(a)]. We adopt the parametrization  $\mathbf{B} = B [\sin(\varphi) \sin(\theta) \mathbf{e}_a + \cos(\varphi) \sin(\theta) \mathbf{e}_b + \cos(\theta) \mathbf{e}_c]$ , where the unit vectors  $\mathbf{e}_a$ ,  $\mathbf{e}_b$ , and  $\mathbf{e}_c$  point along the [11 $\bar{2}$ ], [ $\bar{1}$ 10], and [111] directions, respectively.  $\hat{g} = g^{\alpha, \alpha'}$  represents the anisotropic  $g$  factor, which contains only diagonal entries in the aforementioned directions, specifically  $(g_a, g_b, g_c) = (2.3, 2.3, 1.3)$  [17, 18].

There are many methods, such as finite temperature Lanczos [19] or thermal pure quantum states [20, 21], to

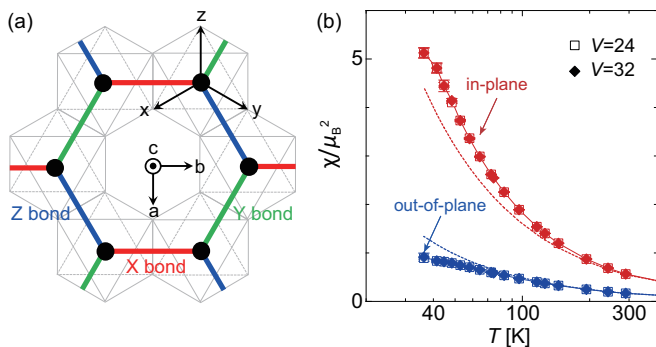


FIG. 1. (a) Schematic of our model for  $\alpha$ -RuCl<sub>3</sub>. Spin-1/2 degrees of freedom,  $\hat{\mathbf{S}}_i$ , are situated on the honeycomb lattice and are subject to first-neighbor Kitaev  $K_1$ , and off-diagonal symmetric  $\Gamma_1$ , exchange interactions, as well as first-neighbor ( $J_1$ ) and third-neighbor ( $J_3$ ) Heisenberg couplings. The RuCl<sub>6</sub> octahedra within the honeycomb lattice, along with the definition of the cubic spin-space axes  $[x, y, z]$  as indicated in the octahedron's top view, are illustrated. (b)  $T$  dependence of the in-plane and out-of-plane uniform spin susceptibilities  $\chi$  from QMC simulations. The dashed line is a fit to Curie's law at high temperatures.

simulate finite temperature properties of the aforementioned Hamiltonian. Here we opt for quantum Monte Carlo (QMC) simulations that excel at thermodynamic quantities. Frustrated spin systems, like Kitaev materials, generically suffer from the infamous negative sign problem that leads to an exponential increase in the required computational power as a function of the volume  $V$  of the system and inverse temperature  $\beta$  [22]. Since the severity of this problem depends on the specific formulations, optimization strategies to alleviate it can be put forward. Indeed, in our recent publication [23], we have developed a fermion QMC approach using the auxiliary-field QMC (AFQMC) algorithm for fermions [24–27] to tackle frustrated spin models. The generalized Kitaev model, describing materials, such as layered iridates and  $\alpha$ -RuCl<sub>3</sub>, benefits from this approach. It mitigates the severity of the negative sign problem and enables QMC simulations at temperatures well below the magnetic exchange scale. This opens up a window of temperatures relevant to experiments. We demonstrate that this method reproduces the experimental magnetotropic susceptibility in  $\alpha$ -RuCl<sub>3</sub> [16]. Hamiltonian (1) was simulated using the AFQMC method of Ref. [23] and we refer the reader to this paper for details of the approach. We use a Trotter discretization in the range  $\Delta\tau \in [0.01, 0.05]$  depending upon the temperature. For this range of  $\Delta\tau$ , the systematic error is contained within our error bars. We simulated lattices with  $L \times L$  unit cells (each containing two spins, i.e.,  $V = 2L^2$  lattice sites on the honeycomb lattice) and periodic boundary conditions.

*Uniform spin susceptibilities.* A key question is

whether our QMC approach allows one to reach temperature scales that are relevant to experiments for Kitaev materials. To determine the lowest accessible temperature, we numerically evaluate the spin susceptibility tensor  $\hat{\chi} = \chi^{\alpha, \alpha'}$ ,

$$\chi^{\alpha, \alpha'}(\mathbf{q}) = \int_0^\beta d\tau \left[ \langle \hat{\mathcal{O}}_{\mathbf{q}}^\alpha(\tau) \hat{\mathcal{O}}_{-\mathbf{q}}^{\alpha'}(0) \rangle - \langle \hat{\mathcal{O}}_{\mathbf{q}}^\alpha \rangle \langle \hat{\mathcal{O}}_{-\mathbf{q}}^{\alpha'} \rangle \right] \quad (3)$$

where  $\hat{\mathcal{O}}_{\mathbf{q}}^\alpha = \frac{\mu_B g^{\alpha, \alpha'}}{\sqrt{V}} \sum_{\mathbf{r}} e^{i\mathbf{q} \cdot \mathbf{r}} \left( \hat{S}_{\mathbf{r}, A}^\alpha + \hat{S}_{\mathbf{r}, B}^\alpha e^{i\mathbf{q} \cdot \mathbf{R}} \right)$ . Here  $\mathbf{r}$  runs over the  $A$  sublattice (or unit cell) and  $\mathbf{R} = 2/3(\mathbf{A}_2 - \mathbf{A}_1/2)$  with the primitive lattice vectors  $\mathbf{A}_1 = (1, 0)$  and  $\mathbf{A}_2 = (\frac{1}{2}, \frac{\sqrt{3}}{2})$ . Projecting  $\chi^{\alpha, \alpha'}(\mathbf{q} = \Gamma)$  onto the in-plane (out-of-plane) direction yields the in-plane (out-of-plane) uniform spin susceptibility  $\chi_{\parallel} = \mathbf{e}_{ab}^T \hat{\chi} \mathbf{e}_{ab}$  ( $\chi_{\perp} = \mathbf{e}_c^T \hat{\chi} \mathbf{e}_c$ ).

Figure 1(b) plots the results down to the lowest accessible temperature. For model parameters proposed to describe  $\alpha$ -RuCl<sub>3</sub> [28],  $(J_1, J_3, K_1, \Gamma_1) = (-5.8, 5.8, -58, 29)$  K, we can reach temperatures down to  $T \sim 30$  K on the relatively large lattice size  $V = 32$ , which is larger than the lattice sizes in exact diagonalization calculations at finite temperature (i.e.,  $V = 24$  sites [19]). On the experimental front,  $\alpha$ -RuCl<sub>3</sub> exhibits zigzag spin order at low temperatures, but proximity to the Kitaev spin liquid suggests that high energy features of this material are described by Majorana fermions [8, 9]. These fermions will hence only show up in finite-temperature properties in an intermediate temperature range bounded by the ordering temperature from below and the coherence scale of the Majorana fermions from above. Experimentally, this temperature range corresponds to  $T \in [10, 100]$  K [8, 9], and it is remarkable to observe that the QMC simulations can access this regime before the negative sign problem becomes too severe. Our numerical results, as a function of decreasing temperature, not only confirm the deviation from a Curie law at high temperatures but also demonstrate a clear trend in  $\chi_{\parallel} > \chi_{\perp}$ , which exhibits similar behavior as experiments in  $\alpha$ -RuCl<sub>3</sub> reported in Refs. [5–7, 13].

*Magnetotropic susceptibility.* We now focus our attention on recent measurements for  $\alpha$ -RuCl<sub>3</sub> concerning the magnetotropic susceptibility over a wide range of temperatures and magnetic fields [16]. This quantity is defined as the second derivative of the free energy with respect to the rotation angle of the magnetic field and is the thermodynamic coefficient associated with the magnetic anisotropy. In our QMC simulations, and as detailed in the Supplemental Material [29], the magnetotropic susceptibility in the rotation plane perpendicular to the unit

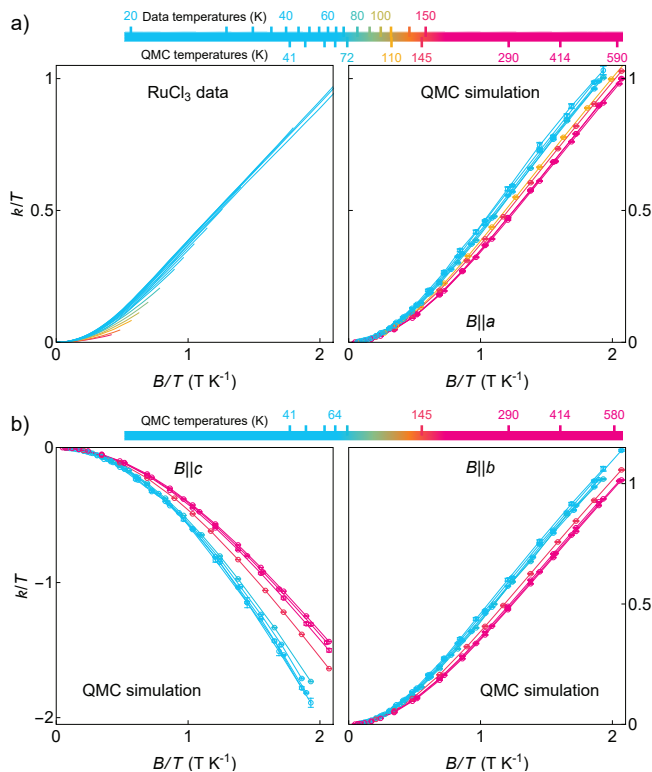


FIG. 2. (a) The magnetotropic susceptibility per Ru atom of  $\alpha$ - $\text{RuCl}_3$  normalized by temperature  $k/T$  versus magnetic field normalized by temperature  $B/T$ . Both  $k$  and  $T$  are given in energy units for the vertical axis, making  $k/T$  a dimensionless quantity.  $T$  is in kelvin for the lower axis. Left panel shows the experimental data from [16] and right panel shows our QMC calculations using the model parameters described in the text. The applied magnetic field is oriented close to the  $\mathbf{a}$ - $\mathbf{b}$  plane. The collapse of blue curves in both the experimental data and the calculated magnetotropic susceptibility appear to show scaling behavior in the temperature range  $T \in [20, 70]$  K. Above this temperature, the experimental data deviates toward the paramagnetic scaling (red curves) observed at high temperatures in the QMC calculations. Limited field range at these temperatures prevents experimental access to the high-temperature scaling regime. (b) Same as (a) for varying magnetic field directions in the QMC calculations.

vector  $\mathbf{e}$  is computed using [30, 31]

$$k = \frac{1}{V} \left[ \mu_B \mathbf{e} \times (\mathbf{e} \times \mathbf{B}) \cdot \hat{\mathbf{g}} \cdot \langle \hat{\mathbf{S}}_{tot} \rangle - \mu_B^2 \int_0^\beta d\tau \left[ \langle (\mathbf{e} \times \mathbf{B}) \cdot \hat{\mathbf{g}} \cdot \hat{\mathbf{S}}_{tot}(\tau) (\mathbf{e} \times \mathbf{B}) \cdot \hat{\mathbf{g}} \cdot \hat{\mathbf{S}}_{tot}(0) \rangle - \langle (\mathbf{e} \times \mathbf{B}) \cdot \hat{\mathbf{g}} \cdot \hat{\mathbf{S}}_{tot} \rangle^2 \right] \right] \quad (4)$$

with  $\hat{\mathbf{S}}_{tot} = \sum_i \hat{\mathbf{S}}_i$  and an imaginary time  $\tau$ . Figure 2 presents the results for the magnetotropic susceptibility  $k$ , with respect to temperature and magnetic field in the  $\mathbf{a}$ - $\mathbf{b}$  plane, and compares them to experiments for  $\alpha$ - $\text{RuCl}_3$  [16]. The magnetotropic susceptibility measure-

ments appear to show temperature and magnetic field scaling behavior of the form  $k = Tf(B/T)$  over the temperature range bounded by the spin ordering temperature and the coherence scale of Majorana fermions,  $T \approx [10, 100]$  K [see the left panel of Fig. 2(a)]. Our QMC data shown in the right panel of Fig. 2(a) quantitatively reproduces this behavior below the magnetic exchange scale. Furthermore, our numerical results suggest that as the temperature increases, there is a departure from the low-temperature scalinglike behavior, and we then observe a more well-defined scaling behavior at high temperatures. The experimental data shows the departure from the low-temperature scalinglike behavior, but higher magnetic fields are required to reach the high-temperature, paramagnetic scaling. Moreover, for the other magnetic field directions in the QMC data, for instance, along the  $\mathbf{c}$  direction [the left panel of Fig. 2(b)] and the  $\mathbf{b}$  direction [the right panel of Fig. 2(b)], the observed behavior remains consistent at both high and low temperatures.

Scaling behavior of the form  $k = Tf(B/T)$  is satisfied for independent local moments for any anisotropic  $g$ -factor (see Supplemental Material [29]). This is expected for any spin system when the temperature exceeds the magnetic exchange energy and the scaling is expected to break down below this energy scale. However, the case of  $\alpha$ - $\text{RuCl}_3$  reveals a more complex scenario. Our QMC data show two behaviors: scaling that is characteristic of a free spin at high temperatures, and an emergent behavior at low temperatures.

To underline the uniqueness of the low-temperature behavior of the magnetotropic susceptibility observed in  $\alpha$ - $\text{RuCl}_3$ , we now compare our findings with other models. Let us start with the pure Kitaev Hamiltonian, as obtained by setting  $\Gamma_1 = J_1 = J_3 = 0$  in Eq. (1) and using the same magnetic field orientation as in Fig. 2(a) [see Figs. 3(a) and 3(b)]. It is remarkable to see that we observe the very same behavior: a well-defined scaling at high temperatures and an emergent low-temperature one, albeit with different numerical values. The temperature at which we observe the crossover between the high and low temperature behavior matches the one at which the uniform spin susceptibility departs from the Curie law. This result confirms the notion that  $\alpha$ - $\text{RuCl}_3$  is proximate to the Kitaev model, and that the low temperature behavior is a distinct property of the Kitaev model.

We now concentrate on a nonfrustrated spin model. To this end we consider for the XXZ model on the honeycomb lattice,  $\hat{H}_s = \sum_{\langle i,j \rangle} J \left[ \hat{S}_i^x \cdot \hat{S}_j^x + \hat{S}_i^y \cdot \hat{S}_j^y \right] + [J + J_z] \hat{S}_i^z \hat{S}_j^z$ , and present QMC results for  $J_z/J = -0.5$  in Fig. 3. As the temperature decreases, the uniform spin susceptibility  $\chi$  deviates from the high-temperature Curie law [see Fig. 3(c)]. In the ferromagnetic case,  $J = -1$ ,  $\chi$  grows and ultimately diverges at low temperatures. As is apparent from the data in Fig. 3(d), our numerical results for the magnetotropic susceptibil-

ity confirm the high-temperature scaling behavior: all curves for  $T/|J| > 10$  collapse when scaled in this way. The breakdown of the data collapse  $k = Tf(B/T)$  agrees with the temperature scale where the deviation from the Curie law behavior is observed in the susceptibility, and the low-temperature data shows no further collapse into a new scaling form. Note that we have checked that the antiferromagnetic case,  $J = 1$ , also exhibits no such recollapse at low temperatures (see Supplemental Material [29]).

*Summary and interpretation.* We have investigated the behavior of the magnetotropic susceptibility,  $k$ , in a realistic magnetic model of  $\alpha$ -RuCl<sub>3</sub> in an external magnetic field. Employing approximation-free, auxiliary-field quantum Monte Carlo simulations, we have explored the rotational anisotropy of the free energy, highlighting the intricate relationship between temperature  $T$ , magnetic field  $B$ , and the unique scaling behavior of  $k$ . Our results show, along with a well-defined scaling behavior at high temperatures,  $k = Tf(B/T)$ , an emergent scaling-like behavior at low temperatures, characterized by a different function,  $f$ . The low-temperature behavior is in quantitative agreement with the experimental data [16] (Fig. 2). The high-temperature scaling, which is inaccessible to experiments, is generic to all spin systems: when

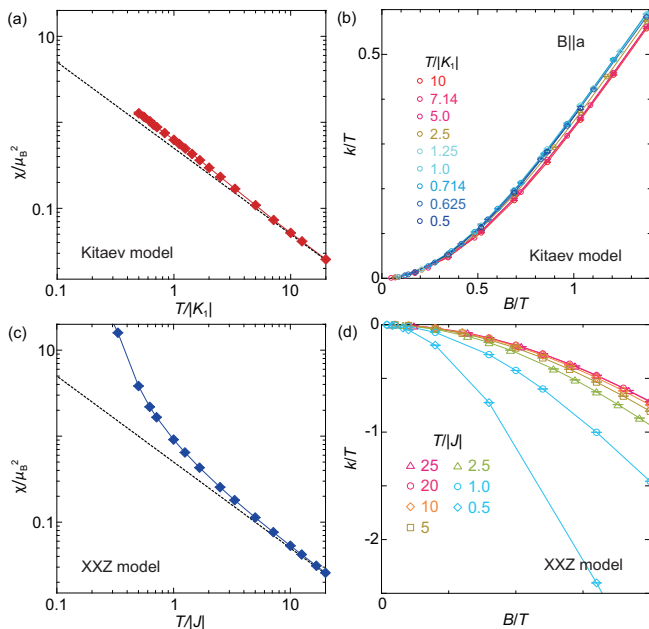


FIG. 3.  $T$  dependence of the uniform spin susceptibilities  $\chi$  (left panels) and the magnetotropic susceptibility normalized by temperature  $k/T$  versus magnetic field normalized by temperature  $B/T$  (right panels). (a), (b) The Kitaev model with  $\Gamma_1 = J_1 = J_3 = 0$  in our model for  $\alpha$ -RuCl<sub>3</sub>, and (c), (d) the unfrustrated spin model on the honeycomb lattice with  $(J, J_z) = (-1, 0.5)$  and  $V = 72$  considered the out-of-plane magnetic-field direction (see the main text). The dashed line represents a fit to Curie's law at high temperatures.

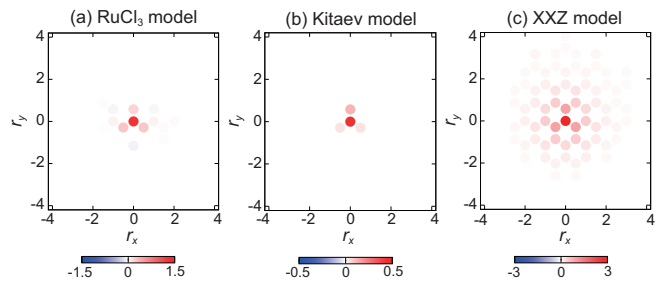


FIG. 4. Real-space torque correlations  $\langle t_r t_0 \rangle = \sum_{\alpha, \gamma} b_\alpha b_\gamma \langle \hat{S}_r^\alpha \hat{S}_0^\beta \rangle$  with  $\mathbf{b} = (\mathbf{e} \times \mathbf{B}) \cdot \hat{\mathbf{g}}$  for the RuCl<sub>3</sub> model (a) [ $T = 41.4$  K and  $B = 5$  T] and the Kitaev model (b) [ $\Gamma_1 = J_1 = J_3 = 0$  in our model for  $\alpha$ -RuCl<sub>3</sub>,  $T/|K_1| = 0.5$  and  $\mu_B B/|K_1| = 0.0579$ ] and the XXZ model with  $(J, J_z) = (-1, 0.5)$  (c) [ $T/|J| = 0.5$  and  $\mu_B B/|J| = 0.1$ ]. Here, the magnetic field is considered in the out-of-plane direction. Note that in the high temperature scaling regime where the temperature is larger than the magnetic exchange coupling, the torque correlations are purely local.

the thermal energy exceeds the magnetic exchange, spin systems behave as independent local moments. The low-temperature behavior, on the other hand, is observed in our model of  $\alpha$ -RuCl<sub>3</sub> as well as in the Kitaev Hamiltonian and is not present for the unfrustrated XXZ model.

The magnetotropic susceptibility relates to the fluctuations of the torque  $\frac{\partial F}{\partial \theta} = \mu_B \sum_i \hat{t}_i$  with  $\hat{t}_i = (\mathbf{e} \times \mathbf{B}) \cdot \hat{\mathbf{g}} \cdot \hat{\mathbf{S}}_i$ . A naive explanation for the emergence of scaling at low temperature would be proximity to a critical point at which long wave length fluctuations of the torque,  $\hat{t}_i$ , become critical and dominate the value of  $k$ . In Fig. 4 we plot the real space fluctuations of  $\hat{t}_i$  both for the model of  $\alpha$ -RuCl<sub>3</sub> at our lowest temperature and for the XXZ model. While torque fluctuations build up for the XXZ model, they remain very short ranged for  $\alpha$ -RuCl<sub>3</sub> and for the Kitaev model [32]. As a consequence, the low-temperature data collapse cannot be understood within a renormalization group approach in which scaling behavior stems from a low-energy effective theory in the vicinity of a critical point.

Instead of being the signature of long-ranged critical torque fluctuations, the observed behavior at low temperatures can be interpreted in terms of the *absence* of such fluctuations beyond the length scale set by the lattice constant and down to temperature scales  $T = 20$  K corresponding to a third of the dominant Kitaev coupling. As a consequence, the adequate model to understand this behavior is that of a renormalized local moment, satisfying  $k = Tf(B/T)$ . Corrections to this model can not be argued away with e.g. a renormalization group argument, and we understand that the scaling has to be approximate.

This point of view places strong constraints on the low lying excitations of Kitaev materials: the magnetotropic susceptibility captures only high energy local

correlations, while the low energy excitations are magnetically isotropic and hence do not contribute to the magnetotropic susceptibility. The qualitative agreement between experimental and numerical data for the Kitaev Hamiltonian supports this point of view. In the Supplemental Material [29] we show that one can formulate, for the Kitaev model, a mean-field theory in which the low lying excitations have no magnetic anisotropy and hence have vanishing torque fluctuations.

Our results lead to a flurry of further applications. We can refine the parameters of the model by fitting numerics to the vast amount angle and temperature dependent data. We have merely looked into the shift of the resonant frequency, corresponding to the real part of the magnetotropic susceptibility. The line-width picks up the energy imaginary part of the response function, that should show unique behavior at, e.g., quantum phase transitions. Finally, a host of other magnetic and metallic materials can and should be investigated with this approach.

We gratefully acknowledge the Gauss Centre for Supercomputing e.V. for funding this project by providing computing time on the GCS Supercomputer SUPERMUC-NG at the Leibniz Supercomputing Centre (project No. pn73xu) as well as the scientific support and HPC resources provided by the Erlangen National High Performance Computing Center (NHR@FAU) of the Friedrich-Alexander-Universität Erlangen-Nürnberg (FAU) under the NHR Project b133ae. NHR funding is provided by federal and Bavarian state authorities. NHR@FAU hardware is partially funded by the German Research Foundation (DFG) – 440719683. T.S. thanks funding from the Deutsche Forschungsgemeinschaft under the Grant No. SA 3986/1-1 as well as the Würzburg-Dresden Cluster of Excellence on Complexity and Topology in Quantum Matter ct.qmat (EXC 2147, Project ID 390858490). F.F.A. acknowledges financial support from the German Research Foundation (DFG) under the grant AS 120/16-1 (Project No. 493886309) that is part of the collaborative research project SFB Q-M&S funded by the Austrian Science Fund (FWF) F 86. K.A.M. thanks financial support from the Austrian Science Fund, SFB F 86, Q-M&S.

---

[1] A. Kitaev, Anyons in an exactly solved model and beyond, *Annals of Physics* **321**, 2 (2006).  
 [2] G. Jackeli and G. Khaliullin, Mott Insulators in the Strong Spin-Orbit Coupling Limit: From Heisenberg to a Quantum Compass and Kitaev Models, *Phys. Rev. Lett.* **102**, 017205 (2009).  
 [3] J. Chaloupka, G. Jackeli, and G. Khaliullin, Zigzag Magnetic Order in the Iridium Oxide  $\text{Na}_2\text{IrO}_3$ , *Phys. Rev. Lett.* **110**, 097204 (2013).

[4] K. W. Plumb, J. P. Clancy, L. J. Sandilands, V. V. Shankar, Y. F. Hu, K. S. Burch, H.-Y. Kee, and Y.-J. Kim,  $\alpha\text{-RuCl}_3$ : A spin-orbit assisted Mott insulator on a honeycomb lattice, *Phys. Rev. B* **90**, 041112 (2014).  
 [5] M. Majumder, M. Schmidt, H. Rosner, A. A. Tsirlin, H. Yasuoka, and M. Baenitz, Anisotropic  $\text{Ru}^{3+} 4d^5$  magnetism in the  $\alpha\text{-RuCl}_3$  honeycomb system: Susceptibility, specific heat, and zero-field NMR, *Phys. Rev. B* **91**, 180401 (2015).  
 [6] J. A. Sears, M. Songvilay, K. W. Plumb, J. P. Clancy, Y. Qiu, Y. Zhao, D. Parshall, and Y.-J. Kim, Magnetic order in  $\alpha\text{-RuCl}_3$ : A honeycomb-lattice quantum magnet with strong spin-orbit coupling, *Phys. Rev. B* **91**, 144420 (2015).  
 [7] Y. Kubota, H. Tanaka, T. Ono, Y. Narumi, and K. Kindo, Successive magnetic phase transitions in  $\alpha\text{-RuCl}_3$ : XY-like frustrated magnet on the honeycomb lattice, *Phys. Rev. B* **91**, 094422 (2015).  
 [8] S.-H. Do, S.-Y. Park, J. Yoshitake, J. Nasu, Y. Motome, Y. S. Kwon, D. T. Adroja, D. J. Voneshen, K. Kim, T. H. Jang, J. H. Park, K.-Y. Choi, and S. Ji, Majorana fermions in the Kitaev quantum spin system  $\alpha\text{-RuCl}_3$ , *Nature Physics* **13**, 1079 (2017).  
 [9] A. Banerjee, J. Yan, J. Knolle, C. A. Bridges, M. B. Stone, M. D. Lumsden, D. G. Mandrus, D. A. Tennant, R. Moessner, and S. E. Nagler, Neutron scattering in the proximate quantum spin liquid  $\alpha\text{-RuCl}_3$ , *Science* **356**, 1055 (2017).  
 [10] I. A. Leahy, C. A. Pocs, P. E. Siegfried, D. Graf, S.-H. Do, K.-Y. Choi, B. Normand, and M. Lee, Anomalous Thermal Conductivity and Magnetic Torque Response in the Honeycomb Magnet  $\alpha\text{-RuCl}_3$ , *Phys. Rev. Lett.* **118**, 187203 (2017).  
 [11] R. Hentrich, A. U. B. Wolter, X. Zotos, W. Brenig, D. Nowak, A. Isaeva, T. Doert, A. Banerjee, P. Lampen-Kelley, D. G. Mandrus, S. E. Nagler, J. Sears, Y.-J. Kim, B. Büchner, and C. Hess, Unusual Phonon Heat Transport in  $\alpha\text{-RuCl}_3$ : Strong Spin-Phonon Scattering and Field-Induced Spin Gap, *Phys. Rev. Lett.* **120**, 117204 (2018).  
 [12] Y. Kasahara, K. Sugii, T. Ohnishi, M. Shimozawa, M. Yamashita, N. Kurita, H. Tanaka, J. Nasu, Y. Motome, T. Shibauchi, and Y. Matsuda, Unusual Thermal Hall Effect in a Kitaev Spin Liquid Candidate  $\alpha\text{-RuCl}_3$ , *Phys. Rev. Lett.* **120**, 217205 (2018).  
 [13] P. Lampen-Kelley, S. Rachel, J. Reuther, J.-Q. Yan, A. Banerjee, C. A. Bridges, H. B. Cao, S. E. Nagler, and D. Mandrus, Anisotropic susceptibilities in the honeycomb Kitaev system  $\alpha\text{-RuCl}_3$ , *Phys. Rev. B* **98**, 100403 (2018).  
 [14] A. Banerjee, P. Lampen-Kelley, J. Knolle, C. Balz, A. A. Aczel, B. Winn, Y. Liu, D. Pajerowski, J. Yan, C. A. Bridges, A. T. Savici, B. C. Chakoumakos, M. D. Lumsden, D. A. Tennant, R. Moessner, D. G. Mandrus, and S. E. Nagler, Excitations in the field-induced quantum spin liquid state of  $\alpha\text{-RuCl}_3$ , *npj Quantum Materials* **3**, 8 (2018).  
 [15] O. Tanaka, Y. Mizukami, R. Harasawa, K. Hashimoto, K. Hwang, N. Kurita, H. Tanaka, S. Fujimoto, Y. Matsuda, E. G. Moon, and T. Shibauchi, Thermodynamic evidence for a field-angle-dependent Majorana gap in a Kitaev spin liquid, *Nature Physics* (2022), 10.1038/s41567-021-01488-6.  
 [16] K. A. Modic, R. D. McDonald, J. P. C. Ruff, M. D.

- Bachmann, Y. Lai, J. C. Palmstrom, D. Graf, M. K. Chan, F. F. Balakirev, J. B. Betts, G. S. Boebinger, M. Schmidt, M. J. Lawler, D. A. Sokolov, P. J. W. Moll, B. J. Ramshaw, and A. Shekhter, Scale-invariant magnetic anisotropy in  $\alpha$ -RuCl<sub>3</sub> at high magnetic fields, *Nature Physics* (2020), 10.1038/s41567-020-1028-0.
- [17] J. Chaloupka and G. Khaliullin, Magnetic anisotropy in the Kitaev model systems Na<sub>2</sub>IrO<sub>3</sub> and  $\alpha$ -RuCl<sub>3</sub>, *Phys. Rev. B* **94**, 064435 (2016).
- [18] R. Yadav, N. A. Bogdanov, V. M. Katukuri, S. Nishimoto, J. van den Brink, and L. Hozoi, Kitaev exchange and field-induced quantum spin-liquid states in honeycomb  $\alpha$ -RuCl<sub>3</sub>, *Scientific Reports* **6**, 37925 (2016).
- [19] S. M. Winter, K. Riedl, D. Kaib, R. Coldea, and R. Valentí, Probing  $\alpha$ -RuCl<sub>3</sub> Beyond Magnetic Order: Effects of Temperature and Magnetic Field, *Phys. Rev. Lett.* **120**, 077203 (2018).
- [20] T. Suzuki and S.-I. Suga, Effective model with strong Kitaev interactions for  $\alpha$ -RuCl<sub>3</sub>, *Phys. Rev. B* **97**, 134424 (2018).
- [21] P. Laurell and S. Okamoto, Dynamical and thermal magnetic properties of the Kitaev spin liquid candidate  $\alpha$ -RuCl<sub>3</sub>, *npj Quantum Materials* **5**, 2 (2020).
- [22] M. Troyer and U.-J. Wiese, Computational Complexity and Fundamental Limitations to Fermionic Quantum Monte Carlo Simulations, *Phys. Rev. Lett.* **94**, 170201 (2005).
- [23] T. Sato and F. F. Assaad, Quantum Monte Carlo simulation of generalized Kitaev models, *Phys. Rev. B* **104**, L081106 (2021).
- [24] R. Blankenbecler, D. J. Scalapino, and R. L. Sugar, Monte Carlo calculations of coupled boson-fermion systems. I, *Phys. Rev. D* **24**, 2278 (1981).
- [25] S. White, D. Scalapino, R. Sugar, E. Loh, J. Gubernatis, and R. Scalettar, Numerical study of the two-dimensional Hubbard model, *Phys. Rev. B* **40**, 506 (1989).
- [26] M. Bercx, F. Goth, J. S. Hofmann, and F. F. Assaad, The ALF (Algorithms for Lattice Fermions) project release 1.0. Documentation for the auxiliary field quantum Monte Carlo code, *SciPost Phys.* **3**, 013 (2017) .
- [27] ALF Collaboration, F. F. Assaad, M. Bercx, F. Goth, A. Götz, J. S. Hofmann, E. Huffman, Z. Liu, F. Parisen Toldin, J. S. E. Portela, and J. Schwab, The ALF (Algorithms for Lattice Fermions) project release 2.0. Documentation for the auxiliary-field quantum Monte Carlo code, *SciPost Phys. Codebases* (2022) .
- [28] S. M. Winter, K. Riedl, P. A. Maksimov, A. L. Chernyshev, A. Honecker, and R. Valentí, Breakdown of magnons in a strongly spin-orbital coupled magnet, *Nature Communications* **8**, 1152 (2017) .
- [29] See the Supplemental Material included below for additional details on the derivation of the magnetotropic susceptibility in our quantum Monte Carlo simulations, the behavior of the magnetotropic susceptibility for independent local moments, the antiferromagnetic case of the XXZ model on the honeycomb lattice, and our mean field calculations for the Kitaev model.
- [30] I. Mandal, Magnetotropic Response in Ruthenium Chloride, *Acta Physica Polonica A* **140**, 372 (2021).
- [31] A. Shekhter, R. D. McDonald, B. J. Ramshaw, and K. A. Modic, Magnetotropic susceptibility, *Phys. Rev. B* **108**, 035111 (2023).
- [32] Note that at temperatures beyond the magnetic exchange, torque correlations vanish between any two dis-

tinct lattice sites.

## SUPPLEMENTARY INFORMATION

### magnetotropic susceptibility

The magnetotropic susceptibility quantifies how the free energy of a system changes as the direction of the magnetic field varies, especially under small rotations. This quantity, denoted as  $k$ , is defined as the second derivative of the free energy with respect to the rotation angle  $\lambda$  of the magnetic field

$$k = \left. \frac{\partial^2 F}{\partial \lambda^2} \right|_{\lambda=0}. \quad (5)$$

Now consider an arbitrary vector  $\mathbf{B}$  representing the magnetic field. Assume that the direction of this vector fluctuates within a plane. This plane is defined by its normal vector  $\mathbf{e}$ . The fluctuations or oscillations occur around the direction of  $\mathbf{B}$ , within the defined plane. To describe these rotations, we employ the generators of SO(3) symmetry, specifically  $e^{i\hat{\mathbf{K}} \cdot \mathbf{e} \lambda}$ . Here,  $\hat{\mathbf{K}}$  consists of purely imaginary entities

$$\begin{aligned} \hat{K}_1 &= \begin{bmatrix} 0 & 0 & 0 \\ 0 & 0 & -i \\ 0 & i & 0 \end{bmatrix}, & \hat{K}_2 &= \begin{bmatrix} 0 & 0 & i \\ 0 & 0 & 0 \\ -i & 0 & 0 \end{bmatrix} \\ \hat{K}_3 &= \begin{bmatrix} 0 & -i & 0 \\ i & 0 & 0 \\ 0 & 0 & 0 \end{bmatrix} \end{aligned} \quad (6)$$

which satisfy the commutation relations  $[\hat{K}_\alpha, \hat{K}_\beta] = i\epsilon_{\alpha\beta\gamma} \hat{K}_\gamma$ . Within this, when the magnetic field is rotated by small angle  $\lambda$ , the total Hamiltonian from the main text is described as

$$\hat{H}(\lambda) = \hat{H}_s - \mu_B e^{i\hat{\mathbf{K}} \cdot \mathbf{e} \lambda} \mathbf{B} \cdot \hat{\mathbf{g}} \cdot \hat{\mathbf{S}}_{tot} \quad (7)$$

with  $\hat{\mathbf{S}}_{tot} = \sum_{i,\alpha} \hat{S}_i^\alpha$ .  $\hat{\mathbf{g}}$  represents the anisotropic  $g$  factor.

The free energy, in relation to the Hamiltonian (7), is given by  $F(\lambda) = -\frac{1}{\beta} \log \text{Tr} \left[ e^{-\beta \hat{H}(\lambda)} \right]$  with the inverse temperature  $\beta$ . We can now expand the Hamiltonian (7) in terms of small  $\lambda$ , giving

$$\hat{H}(\lambda) = \hat{H}_s + \hat{H}_1(\lambda) + O(\lambda^2). \quad (8)$$

Here, the term  $\hat{H}_1$  captures the second-order effects of the rotation, and is given by

$$\hat{H}_1 = -\mu_B \left[ i\hat{\mathbf{K}} \cdot \mathbf{e} \lambda + \frac{(i\hat{\mathbf{K}} \cdot \mathbf{e})^2}{2} \lambda^2 \right] \mathbf{B} \cdot \hat{\mathbf{g}} \cdot \hat{\mathbf{S}}_{tot}. \quad (9)$$

This expansion allows to express the second derivative of the free energy with respect to the rotation angle  $\lambda$  in

terms of  $\hat{H}_1$

$$\begin{aligned} \left. \frac{\partial^2 F}{\partial \lambda^2} \right|_{\lambda=0} &= \left\langle \frac{\partial^2 \hat{H}_1}{\partial \lambda^2} \right\rangle \\ &- \int_0^\beta d\tau \left[ \left\langle \frac{\partial \hat{H}_1(\tau)}{\partial \lambda} \frac{\partial \hat{H}_1(0)}{\partial \lambda} \right\rangle - \left\langle \frac{\partial \hat{H}_1}{\partial \lambda} \right\rangle \left\langle \frac{\partial \hat{H}_1}{\partial \lambda} \right\rangle \right]. \end{aligned} \quad (10)$$

The integration runs over an imaginary time  $\tau$ . Taking the first and second derivatives of  $\hat{H}_1$  in Eq. (9), we obtain

$$\begin{aligned} \left. \frac{\partial \hat{H}_1}{\partial \lambda} \right|_{\lambda=0} &= -\mu_B (i\hat{\mathbf{K}} \cdot \mathbf{e}) \cdot \mathbf{B} \cdot \hat{\mathbf{g}} \cdot \hat{\mathbf{S}}_{tot} \\ &= \mu_B (\mathbf{e} \times \mathbf{B}) \cdot \hat{\mathbf{g}} \cdot \hat{\mathbf{S}}_{tot}, \\ \left. \frac{\partial^2 \hat{H}_1}{\partial \lambda^2} \right|_{\lambda=0} &= \mu_B (i\hat{\mathbf{K}} \cdot \mathbf{e})^2 \cdot \mathbf{B} \cdot \hat{\mathbf{g}} \cdot \hat{\mathbf{S}}_{tot} \\ &= \mu_B \mathbf{e} \times (\mathbf{e} \times \mathbf{B}) \cdot \hat{\mathbf{g}} \cdot \hat{\mathbf{S}}_{tot}. \end{aligned} \quad (11)$$

Synthesizing Eqs. (10) and (11), the expression for the magnetotropic susceptibility  $k$  is

$$\begin{aligned} k &= \frac{1}{V} \left[ \mu_B \mathbf{e} \times (\mathbf{e} \times \mathbf{B}) \cdot \hat{\mathbf{g}} \cdot \langle \hat{\mathbf{S}}_{tot} \rangle \right. \\ &- \mu_B^2 \int_0^\beta d\tau \left[ \langle (\mathbf{e} \times \mathbf{B}) \cdot \hat{\mathbf{g}} \cdot \hat{\mathbf{S}}_{tot}(\tau) (\mathbf{e} \times \mathbf{B}) \cdot \hat{\mathbf{g}} \cdot \hat{\mathbf{S}}_{tot}(0) \rangle \right. \\ &\left. \left. - \langle (\mathbf{e} \times \mathbf{B}) \cdot \hat{\mathbf{g}} \cdot \hat{\mathbf{S}}_{tot} \rangle^2 \right) \right] \end{aligned} \quad (12)$$

with lattice sites  $V$ . Within our QMC simulations, this form is employed to compute the magnetotropic susceptibility.

### Properties of the magnetotropic susceptibility in free spin systems

The main text references the temperature-magnetic field scaling behavior of the form  $\beta k = f(\beta B)$  for free spins. Now consider  $\hat{H}_s = 0$  in the Hamiltonian of Eq. (7). In this case, the system is dominated solely by the external magnetic field and temperature. The corresponding free energy is then described by

$$\begin{aligned} F(\lambda) &= -\frac{1}{\beta} \log \text{Tr} \left[ e^{\beta B \mu_B R(\mathbf{e}, \lambda) \mathbf{n} \cdot \hat{\mathbf{g}} \cdot \hat{\mathbf{S}}_{tot}} \right] \\ &= -\frac{1}{\beta} g(\beta B, \lambda). \end{aligned} \quad (13)$$

Here,  $R(\mathbf{e}, \lambda) = e^{i\hat{\mathbf{K}} \cdot \mathbf{e} \lambda}$  represents the rotation matrix in the presence of the magnetic field, and  $\mathbf{B} = B \mathbf{n}$  with  $\mathbf{n}$  being the unit vector pointing in the direction of the magnetic field. This simplified expression for the free energy provides an explicit link between the rotation angle and the behavior of the system under a magnetic field.

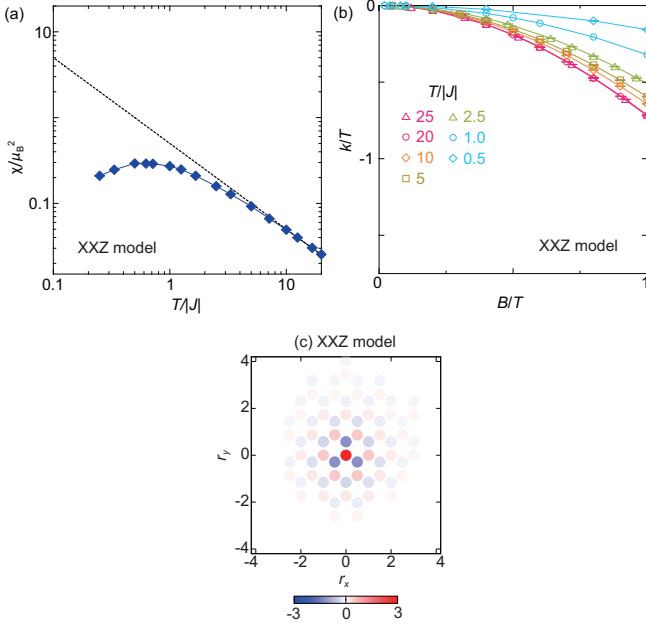


FIG. 5. QMC results for the XXZ model on the honeycomb lattice with  $(J, J_z) = (1, -0.5)$ . (a)  $T$  dependence of the uniform spin susceptibilities  $\chi$ . The dashed line represents a fit to Curie's law at high temperatures. (b) The magnetotropic susceptibility normalized by temperature  $k/T$  versus magnetic field normalized by temperature  $B/T$  and (c) real-space torque correlations  $\langle t_r t_0 \rangle$  [ $T/|J| = 0.5$  and  $\mu_B B/|J| = 0.1$ ]. The magnetic field is considered in the out-of-plane direction. Here,  $V = 72$  lattice.

Taking this forward, the magnetotropic susceptibility  $k$  in this context is given by

$$k = \left. \frac{\partial^2 F(\lambda)}{\partial \lambda^2} \right|_{\lambda=0} = -\frac{1}{\beta} \left. \frac{\partial^2 g(\beta B, \lambda)}{\partial \lambda^2} \right|_{\lambda=0}. \quad (14)$$

Upon further simplification, we arrive at the key relationship:

$$\beta k = f(\beta B). \quad (15)$$

This equation accentuates the intricate relationship between the temperature and magnetic field strength.

### Magnetotropic susceptibility for the XXZ model

In the main text, we consider the ferromagnetic case of the XXZ model on the honeycomb lattice. Now QMC results for the antiferromagnetic case,  $(J, J_z) = (1, -0.5)$ , are presented in Fig. 5. As the temperature decreases, the uniform spin susceptibility,  $\chi$ , deviates from the high-temperature Curie law (see Fig. 5(a)). Local antiferromagnetic correlations lead to a suppression of  $\chi$

with respect to the high-temperature Curie law, and at low temperatures,  $\chi$  will scale to a constant value, reflecting the presence of Goldstone modes. Figure 5(b) shows the magnetotropic susceptibility  $k$ . It shares the same features as for the ferromagnetic case shown in the main text. Our numerical data confirm the data collapse  $k = T f(B/T)$  for  $T/|J| > 10$  and its breakdown agrees with the temperature scale where the deviation from Curie law behavior is observed in  $\chi$ . Figure 5(c) plots the torque correlations. As is apparent, torque fluctuations build up.

### Abrikosov fermion representation and mean-field ansatz for the Kitaev model

The Kitaev model consists of  $S = 1/2$  spins on a honeycomb lattice with Hamiltonian

$$\hat{H} = K_1 \sum_{i \in A, \alpha} \hat{S}_i^\alpha \hat{S}_{i+\delta_\alpha}^\alpha. \quad (16)$$

Here  $i$  runs over the A sublattice and  $i + \delta_\alpha$  with  $\alpha = (1, 2, 3)$  over the first neighbors. Now we represent the spin-1/2 degree of freedom  $\hat{S}_i^\alpha$  in terms of Abrikosov fermions

$$\hat{S}_i^\alpha = \frac{1}{2} \sum_{s, s'} \hat{f}_{i,s}^\dagger \sigma_{s,s'}^\alpha \hat{f}_{i,s'} \quad (17)$$

with the local constraint  $\sum_s \hat{f}_{i,s}^\dagger \hat{f}_{i,s} = 1$ .  $s$ - corresponds to a spin index and  $\sigma$  corresponds to the vector of Pauli spin-1/2 matrices.

Using a Fierz transformation an exact rewriting of the Kitaev model reads:

$$\begin{aligned} \hat{H}_{\text{Kitaev}} = & -\frac{K_1}{8} \sum_{i \in A, \gamma} \left( \hat{D}_{i, i+\delta_\gamma} \hat{D}_{i, i+\delta_\gamma}^\dagger + \hat{D}_{i, i+\delta_\gamma}^\dagger \hat{D}_{i, i+\delta_\gamma} \right) \\ & -\frac{K_1}{8} \sum_{i \in A, \gamma} \left( \hat{D}_{i, i+\delta_\gamma}^\gamma \hat{D}_{i, i+\delta_\gamma}^{\gamma\dagger} + \hat{D}_{i, i+\delta_\gamma}^{\gamma\dagger} \hat{D}_{i, i+\delta_\gamma}^\gamma \right) \end{aligned} \quad (18)$$

with

$$\hat{D}_{i, i+\delta_\gamma} = \sum_s \hat{f}_{i,s}^\dagger \hat{f}_{i+\delta_\gamma, s} \quad (19)$$

and

$$\hat{D}_{i, i+\delta_\gamma}^\gamma = \sum_{s, s'} \hat{f}_{i,s}^\dagger \sigma_{s,s'}^\gamma \hat{f}_{i+\delta_\gamma, s'}. \quad (20)$$

$\hat{D}_{i,j}$  accounts for a spin-independent hopping between sites  $i, j$  such that  $\hat{D}_{i,j} \hat{D}_{i,j}^\dagger$  corresponds to an spin independent or SU(2) invariant exchange process.  $\hat{D}_{i,j}^\gamma$  accounts for spin-flip processes and encodes the magnetic anisotropy of the Kitaev model. A mean field Ansatz that

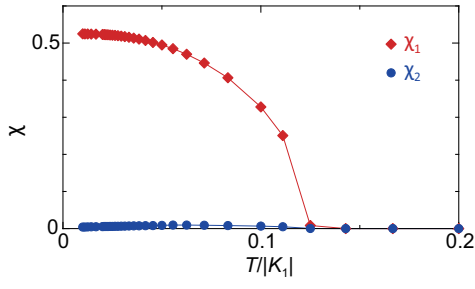


FIG. 6. Abrikosov fermionic mean-field results in the Kitaev model. Here,  $\chi_1 = \langle \hat{D}_{i,i+\delta_\gamma}^\dagger \rangle$  and  $i\chi_2 = \langle \hat{D}_{i,i+\delta_\gamma}^{\gamma\dagger} \rangle$ .

does not break any symmetries of the original Hamiltonian and leads to a mean field description of a spin liquid reads:  $\chi_1 = \langle \hat{D}_{i,i+\delta_\gamma}^\dagger \rangle$ , and  $i\chi_2 = \langle \hat{D}_{i,i+\delta_1}^{\gamma\dagger} \rangle$ , where both  $\chi_1$  and  $\chi_2$  are real. The result of the mean-field self-consistent equations are shown in Fig. 6. At high temperatures, both mean-field order parameters vanish accounting for the high temperature independent local moment regime. At low temperatures,  $\chi_1$  and  $\chi_2$  develop finite expectation values, but with  $\chi_1 \gg \chi_2$ .